Journal of Radioanalytical and Nuclear Chemistry (2021) 328:325–338
https://doi.org/10.1007/s10967-021-07633-y

Gold nanoparticles for ^{99m}Tc-doxorubicin delivery: formulation, in vitro characterization, comparative studies in vivo stability and biodistribution

D. M. El-Safoury[1] · Ahmed B. Ibrahim[1,2] · D. A. El-Setouhy[3] · O. M. Khowessah[3] · M. A. Motaleb[1] · Tamer M. Sakr[2,4]

Received: 6 December 2020 / Accepted: 5 February 2021 / Published online: 25 February 2021

Abstract

The [^{99m}Tc]Tc-Doxorubicin–Gold Nanoparticles (^{99m}Tc-Dox-AuNPs) was formulated as a nanoradiopharmaceutical by different loading procedures to enhance tumor targeting. The formula F1 that was prepared by direct loading of pre-prepared [^{99m}Tc]Tc-Doxorubicin showed a reasonable in-vitro characterization values, high entrapment efficiency ($92 \pm 0.72\%$), acceptable in vitro release data and convenient in-vitro serum stability up to 24 h. F1 presented high tumor uptake (54%ID/g) with high Target/ Non Target (T/NT) (≈ 77) and Drug Target Efficiency percent (%DTE) above 100% at 0.5 h via intratumoral injection that prove the increasing of tumor targeting and in-vivo stability by direct loading for pre-prepared [^{99m}Tc]Tc-Doxorubicin.

✉ Ahmed B. Ibrahim
Ahmed_Badr1981@yahoo.com

✉ Tamer M. Sakr
Tamer_Sakr78@yahoo.com

1 Labeled Compounds Department, Hot Labs Center, Egyptian Atomic Energy Authority, Cairo 13759, Egypt

2 Radioisotopes Production Facility, Second Egyptian Research Reactor Complex, Egyptian Atomic Energy Authority, Cairo 13759, Egypt

3 Pharmaceutics and Industrial Pharmacy Department, Faculty of Pharmacy, Cairo University, Cairo 11562, Egypt

4 Radioactive Isotopes and Generator Department, Hot Labs Center, Egyptian Atomic Energy Authority, Cairo 13759, Egypt

Graphic abstract

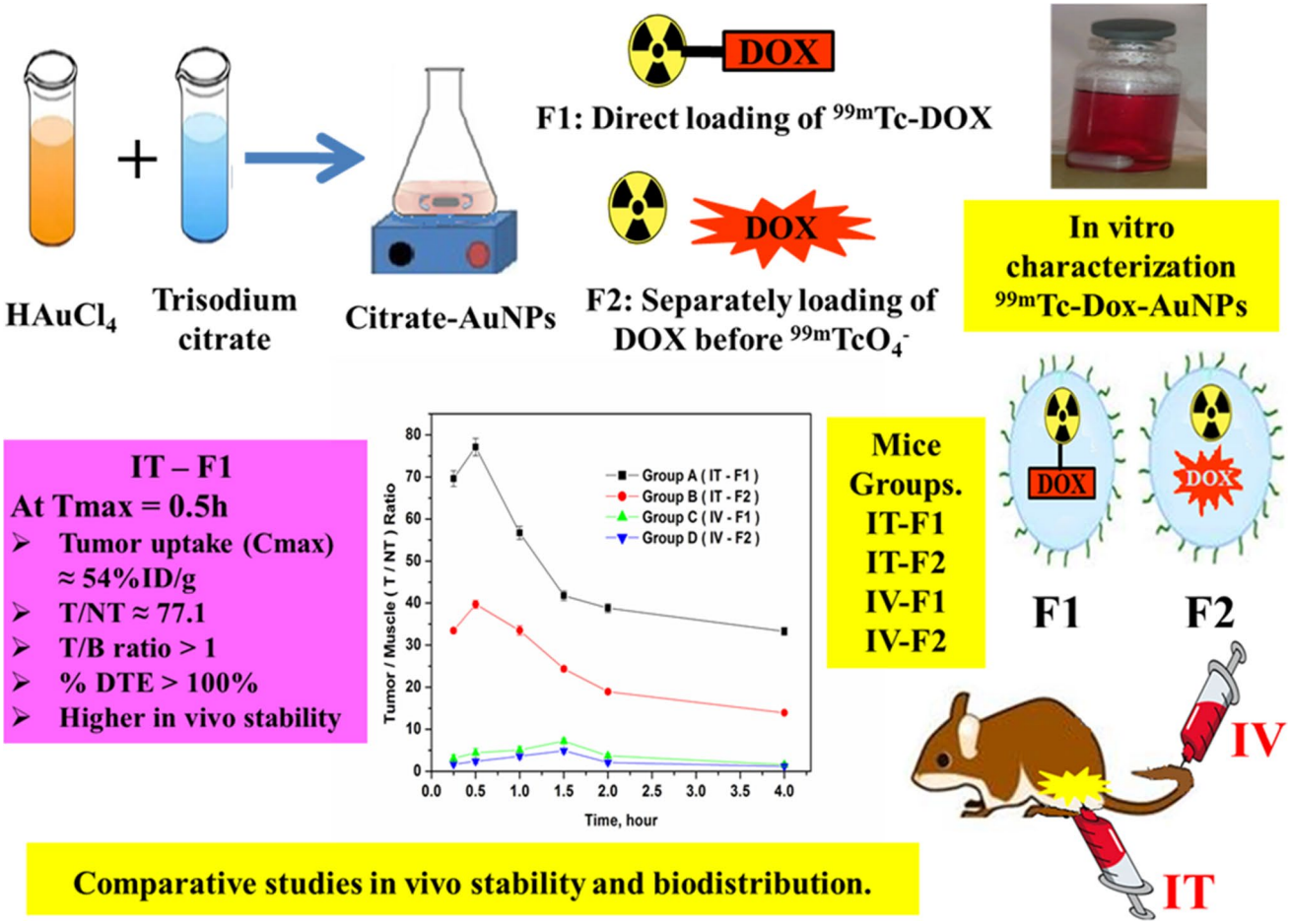

Keywords Gold nanoparticles · [^{99m}Tc]Tc-Doxorubicin · Direct formulation method · Intra-tumoral (IT) · In vivo stability and tumor imaging

Introduction

Nanotechnology, a revolutionary widely used technology, interlinks research in chemistry, physics, engineering, biology and medicine [1]. Development in nanotechnology was increased for medical purposes as drug delivery to target sites, diagnosis and therapeutic purposes for many diseases [2]. Therefore, the use of nanotechnology applications in many diseases, including cancer, aims at early detection and prevention of disease or at improving diagnosis, treatment and follow-up [3]. This technology enhances the use of gold nanoparticles (AuNPs) as a drug nanocarrier for targeted drug delivery to overcome the limits of conventional formulations [4]. AuNPs also named as a highly tunable material [5] and possess unique chemical and physical properties for carrying and delivering the pharmaceuticals. Gold nanoparticles highly multifunctional platforms have several advantages that are greatly beneficial to the formation of drug delivery systems such as chemical static and biocompatibility of basic materials for AuNPs [6] and also its unique nanoscale dimension which provides a large and readily available space for loading target molecules or specific biomarkers to drug delivery systems [7]. Gold colloids are manufactured with a narrow size distribution using environmental-friendly Turkevich method one of the common chemical synthesis technique, to prepare dilute solutions of moderately stable spherical AuNPs, by reducing gold salt ($HAuCl_4$) in aqueous media using citrate ions (reducing and stabilizing agent) at boiling temperature [8]. A ruby red color indicates formation of spherical AuNPs which varies according to their size [9] and is quantitatively explained by the reflection of electromagnetic waves from gold nanoparticles. Transmission electron microscopy, zetasizer and spectrophotometer are used in the characterization morphology, size, and shape of synthesized AuNPs [10]. Characterizations of

gold nano carriers with respect to morphological characteristics, particle size and zeta potential, are very critical to control their desired in vitro and in vivo behavior.

Cancer remains the most deadly disease to haunt mankind in the world today.

The inability to deliver a drug to cancer cells without causing any toxicity to healthy tissues is one of the main causes of the high mortality rate. Therefore a drug-targeting system must be developed to overcome the biological barriers associated with conventional chemotherapy and to selectively target the cancer cell. For instance, gold nanoparticles are concentrated in cancer cells either in a passive way (enhancing permeability and retention effect, EPR) or by active targeting, both of which enhance the concentration of chemotherapy in cancer cells while avoiding the harmful effect on normal cells, thus achieving optimal drug delivery. Doxorubicin (Fig. 1) is a widely used antineoplastic agent in cancer therapy but in clinical applications this anti-cancer drug is limited due to its high cardiotoxicity [11]. Binding doxorubicin with AuNPs could decrease cytotoxicity and at the same time increase the drug bioavailability in cancer cells. Drug interaction with gold nanoparticles can be achieved either by direct linkage between drug and AuNPs or by drug linkage with surface modified gold nanoparticles [12]. The in vivo administration of radiopharmaceutical (the main tool for molecular imaging in nuclear medicine) loaded AuNPs formulation provides an accurate tracking of the biological distribution [13]. The most popular used radioactive isotope in preparation of 85% of radiopharmaceuticals is technetium-99 m (gamma emitter) due to its characteristic properties like its relatively short half-life (6.02 h), convenient γ-ray energy (140 keV) suitable for imaging by gamma camera, low cost and good availability [14]. Pardeep Kumar et al. studies [15, 16] presented the characterization of [^{99m}Tc] Tc-doxorubicin complex by using proton-nuclear magnetic resonance (1H-NMR) and chromatography techniques and the results illustrated that the Doxorubicin has carboxyl, amine, and amide groups that form coordinate bonds with [^{99m}Tc] and satisfy the octahedral geometry of [^{99m}Tc] (III). Formulation of a successful nanoradiopharmaceutical is the most effective way to improve early prognosis of tumors. The formulation of gold nanoparticles with technetium-99 m and doxorubicin depend on the loading procedure that may effect on the biodistribution and in vivo stability. The study aimed to formulate gold nanoparticles as a delivery system of radiopharmaceuticals (^{99m}Tc-Dox) to be used in tumor diagnosis and in vivo evaluation of prepared formulations and different routes of to fully understand their pharmacokinetics and interaction in living biological systems.

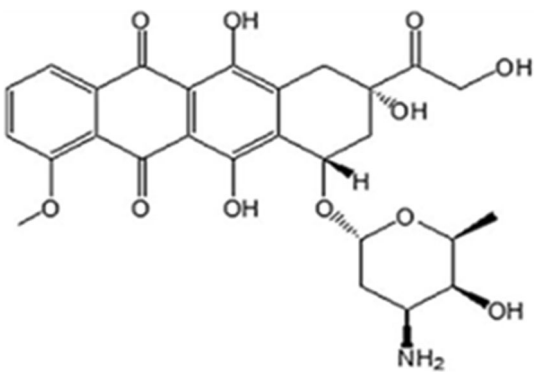

Fig. 1 Doxorubicin chemical structure

Materials and methods

Materials

Commercially available reagents have been used and are not re-purified upon delivery. Double distilled water (kept away from any photochemical responses) is used in all steps related to solution preparation. Hydrogen tetrachloroaurate ($(HAuCl_4)$, M.Wt = 393.83 g/mol) and Doxorubicin hydrochloride **D1515** ($C_{27}H_{29}NO_{11}$.HCl, M.Wt = 579.98 g/mol) were purchased from Sigma-Aldrich Company (St. Louis, Mo), USA. Fetal Bovine serum (FBS) was purchased from Lonza, Bornem, Belgium. Spectra/ Por© semi-permeable membrane tubing (12,000–14,000 Mwt cutoff) was purchased from Spectrum Laboratories Inc. (Rancho Dominguez, CA). Other chemicals and solutions (of analytical grade) were purchased from Merck Co. Whatman paper No.1 sheets were purchased from Merck (Darmstadt, Germany). Sterile Millipore filters (Millipore Co., Bedford, MA, USA). A fresh solution of aquaregia (HNO_3/HCl) (3:1 v/v) was used to clean all used glassware, followed by washing them completely with double distilled water and drying them before use. Technetium 99 m was obtained in the form of pertechnetate elute ([^{99m}Tc]TcO_4^-) from the ^{99}Mo / ^{99m}Tc generator that was manufactured in the Radioisotope Production Facility (RPF) of the Egyptian Atomic Energy Authority (EAEA).

Preparation of gold nanoparticles delivery system (citrate-reduced gold nanoparticles)

A delivery system of **citrate-reduced gold nanoparticles** (citrate-AuNPs) was prepared by reducing hydrogen tetrachloroaurate ($HAuCl_4$) with trisodium citrate ($Na_3C_6H_5O_7$) according to an environmental-friendly synthesis method (Turkevich method) with some modifications. This technique yields fairly uniform size colloids with diameter of 10–20 [8]. In a brief, 1 ml of 1% trisodium citrate (5 mg/ml) was added to a solution of 3 mM $HAuCl_4$ in double

distilled water (1 mg/ml) at 100 °C with continuous simultaneous stirring using magnetic stirring at 500 rpm. The color of the solution mixture changed gradually from yellow to colorless, then to pale grey, turns pale purple and slowly turn into a ruby red color over 10 mi. Turning the solution into deep red color indicates gold nanoparticles formation in the optimum nano size, and here the heating was stopped [9, 17]. After separation of citrate-AuNPs by a centrifuge, the separated citrate-AuNPs were re-dispersed in deionized water for in vitro characterization studies. For further uses, this solution was kept at 4 °C.

In vitro characterization of citrate-gold nanoparticles

Identification of citrate-gold nanoparticles

The identification of gold nanoparticles delivery system was done depending on the gold nanoparticles' electrons interaction with light generates unique optical properties called surface plasmon resonance and the particular wavelength of light where this phenomenon occurs is strongly dependent on the gold nanoparticle size, shape, surface and agglomeration state [18, 19]. Therefore, UV/Vis spectroscopy is used to measure the wavelength of the maximum absorption (λmax) and to confirm the formation of gold nanoparticles that have a single absorption peak in the visible range between 510–550 nm. λmax is re-measured again after 4 months of storage at room temperature and a possible change in max is observed.

Determination of particle size (PS), polydispersity index (PDI), and zeta potential (ZP)

The Zetasizer Nano ZS-90 instrument (Malvern Instruments, Worcestershire, UK) was utilized to determine the PS, PDI, and ZP of citrate-AuNPs. It examines the fluctuations in light scattering due to Brownian movement of particles [20]. Measurement was carried out by diluting 1 ml of citrate-AuNPs with 9 ml of distilled water (10X) to give an appropriate scattering intensity and placing it into a quartz cuvette at 25 ± 0.5 °C, at 90° to the incident beam using a Zetasizer Nano ZS (Malvern Instruments Ltd., Worcestershire, UK). The ZP determines the nanoparticles movement in an electrical field [21].

Morphologic examination

The Morphology and core size of the citrate-AuNPs were investigated using Transmission Electron Microscopy (TEM). One drop of citrate-AuNPs dispersion was settled on a copper grid and left for dry until thin film formation. The film was stained and examined by TEM (JEOL, JEM-100CX, Tokyo, Japan) operated at an accelerating voltage of 200 kV and magnification power of × 100,000 [22].

Preparation of radiolabeled Doxorubicin ([^{99m}Tc] Tc-Doxorubicin complex)

The [^{99m}Tc]Tc-Doxorubicin complex (^{99m}Tc-Dox) was used in formulation of ^{99m}Tc-Dox-AuNPs. The [^{99m}Tc] Tc-Doxorubicin complex was prepared by direct labeling method using sodium dithionite as a reducing agent [23, 24]. The factors (Doxorubicin amount, sodium dithionite, pH and reaction time) affecting on the radiolabeling process were optimized to achieve the maximum radiochemical yields. The doxorubicin solution (2 mg/1 ml) containing different amount of doxorubicin (0.2—1 mg) were dispersed in 1 ml of phosphate buffer at different pH values (3–10) in 10 ml penicillin clean vials. The reducing agent sodium dithionite ($Na_2S_2O_4$) solution (200 mg/ml) was added in amounts ranging from 10 to 50 mg followed by 100 µl of freshly eluted technetium pertechnetate ([^{99m}Tc]TcO_4^-, 400 MBq) eluted from ^{99}Mo/^{99m}Tc generator was added to each vial. Then, the reaction time (5–60 min) was optimized to achieve the maximum radiochemical yield % (RCY) at ambient temperature [25, 26]. Ascending paper chromatography (PC) analysis was used to evaluate the radiochemical yield by using strips of Whatman No. 1 paper chromatography (13 cm in length and 0.5 cm in width) marked at a distance of 2 cm from the lower end and lined into Sect. 1 cm each up to 10 cm. In one strip an amount of 1–2 µl of the reaction solution was seeded (using hypodermic syringe) and was left to develop in an ascending manner in a closed jar containing acetone from which the percent free [^{99m}Tc]TcO_4^- was determined, while the other strip was developed with a mixture of ethanol: water: ammonium hydroxide (2:5:1) from which the percent reduced hydrolyzed [^{99m}Tc]Tc colloid was determined [24]. After complete development, both strips were dried and cut into fragments then the sections were assayed in a NaI(Tl) γ-ray scintillation counter. The percent of [^{99m}Tc]Tc-Doxorubicin complex, free pertechnetate ([^{99m}Tc]TcO_4^-), and reduced hydrolyzed technetium (colloid) were determined using the following Eq. (1):

$$^{99m}\text{Tc} - \text{Doxorubicin complex}\% = 100 - \left(\text{Free}^{99m}\text{TcO}_4^-\% + \text{Colloid }\%\right) \quad (1)$$

Formulation of ^{99m}Tc-Dox-AuNPs

The different formulations (F1 and F2) of ^{99m}Tc-Dox-AuNPs were designed by different loading procedure. F1 was prepared by direct formulation method through

loading different volumes of [^{99m}Tc]Tc-Doxorubicin complex [27] and F2 was prepared by loading different volume of doxorubicin then loading 100 µl of freshly eluted technetium pertechnetate ([^{99m}Tc]TcO_4^-, 400 MBq) [28]. The loading volumes in F1 and F2 were added with magnetic stirring to a fixed volume (1 ml) of citrate-AuNPs to evaluate the maximum amount of doxorubicin that can be loaded on it without any change in color. After development of ^{99m}Tc-Dox-AuNPs, the formulations (F1 and F2) were filtered to get rid of the colloid which was formed during the radiolabeling process through sterile millipore filter (0.2 mm) and the radiochemical yield was assessed using paper chromatography [29].

In vitro evaluation of formulated ^{99m}Tc-Dox-AuNPs

Determination of loading capacity and entrapment efficiency

The 0.1 ml of performed [^{99m}Tc]Tc-Doxorubicin complex (1.5 mg/ ml) was loaded in 1 m) of citrate-AuNPs for preparation F1 but F2 was prepared by separately loading 0.15 ml of doxorubicin solution (2 mg/ml) and 100 µl [^{99m}Tc]TcO_4^- with 1 ml citrate-AuNPs. The dispersion was continuous magnetically stirred for 30 min. the formulations (F1 and F2) of ^{99m}Tc-Dox-AuNPs were segregated by centrifugation. After separation of ^{99m}Tc-Dox-AuNPs formulations (F1 and F2), the remaining doxorubicin (DOX*free*) was detected spectrophotometrically (Shimadzu UV 1700 spectrophotometer, Kyoto, Japan) at 480 nm for F1and F2. The loading capacity and entrapment efficiency percent (EE %) of doxorubicin were determined according the following Eqs. (2, 3) [27, 30]:

$$\text{Loading capacity of DOX (mg/mg)} = \left(\left[\text{DOX}_\text{i}\right] - \left[\text{DOX}_\text{free}\right]\right)/\text{M}_\text{carrier} \quad (2)$$

$$\text{Entrapment Efficiency of DOX (\%)} = \left(\left(\left[\text{DOX}_\text{i}\right] - \left[\text{DOX}_\text{free}\right]\right)/\left[\text{DOX}_\text{i}\right]\right) \times 100 \quad (3)$$

where [DOX_i] and [DOX_{free}] are the initial DOX content and free DOX content in supernatant, respectively and $M_{carrier}$ is the weight of citrate-AuNPs.

In-vitro release study

The doxorubicin release from prepared formulations (^{99m}Tc-Dox-AuNPs) was evaluated using the membrane diffusion techniques [31], in triplicate, at 37 ± 0.5 °C and 50 rpm shaker water bath. According to the EE %, the calculated volumes of ^{99m}Tc-Dox-AuNPs containing same amount of the doxorubicin were placed in tubing with Spectra Por© semi-permeable membrane at both sides. The tube was immersed in 50 ml release medium of phosphate buffer solution (pH 5) [27]. Samples of 3 ml of the release medium were withdrawn at designed time intervals (0.25—8 h) and immediately replaced with freshly same volume of release medium [32]. The cumulative doxorubicin release percentage were calculated and plotted against time to determine the t_{50} and Q8h.

Table 1 Biodistribution experimental design

A	Mice were injected intratumoral(IT) with 0.1 ml of F1 (IT-F1)
B	Mice were injected intratumoral (IT) with 0.1 ml of F2 (IT-F2)
C	Mice were injected intravenous (IV) with 0.1 ml of F1 (IV-F1)
D	Mice were injected intravenous (IV) with 0.1 ml of F2 (IV-F2)

In-vitro stability study in mice serum

In order to prove effectiveness of ^{99m}Tc-Dox-AuNPs as a potential radiopharmaceutical and ensure that the radiolabeling process is stable in physiological conditions [33], we studied in-vitro stability of ^{99m}Tc-Dox-AuNPs in mice serum by incubating 100 µl of formulations (F1 and F2) separately, in 900 µl mice serum at 37 °C up to 24 h and the radiochemical yields were assessed by ascending paper chromatographic method [34] at 0, 0.25, 0.5, 1.5, 2, 3 and 24 h post-incubation.

Biodistribution studies

^{99m}Tc-Dox-AuNPs biodistribution studies were carried out in compliance with the recommendations of the Animal Ethics Committee and with the guidelines of the Egyptian Atomic Energy Authority. The animal experiments complied with the National Institutes of Health guide for the care and use of laboratory animals (NIH Publications No. 8023, revised 1978). The protocol of the studies was approved by Research Ethics Committee for experimental and clinical studies, Faculty of Pharmacy, Cairo University, Egypt (REC-FOPC)—(Approval No. PI 1265).

Solid tumor induction in mice

The biodistribution of ^{99m}Tc-Dox-AuNPs formulation was studied in Swiss albino mice infected with solid tumors prepared by taking the parent tumor line (Ehrlich Ascites Carcinoma) from 7-day-old donor female Swiss albino mice and diluted with sterile physiological saline solution to ensure tumor formation to give 12.5×10^6 cells/ml. Then, about 0.2 ml of this solution was injected intramuscularly in the right thigh of the Swiss albino mice weighing 20–30 g to produce solid tumor and the left leg being taken as control and the animals were maintained until the tumor progression appeared this takes about 10–15 days. It has been proven that the use of Ehrlich Ascites Carcinoma (EAC) as a solid

tumor model in chemotherapy research gives accurate and reliable results [35, 36].

Biodistribution assay

Solid tumor bearing albino mice of body mass 20–30 gm were classified into four groups A, B, C and D (18 mice/group) as in Table 1. Three mice per each time point for each route of injection. 100 µl of formulated ^{99m}Tc-Dox-AuNPs F1 and F2 containing 185–1850 kBq was intratumoraly injected in group A and B, respectively and intravenously injected in groups C and D, respectively. Mice housed in divided separated groups of three and provided with food and water [37]. At predetermined time intervals 15, 30, 60, 90, 120, 240 min post IV & IT injection the animals were weighed, anesthetized by chloroform and dissected. The desired organs and tumor were collected after dissection, weighed and washed with normal saline then transferred into counting vials [38]. Blood samples were obtained by puncture of the heart with hypodermic syringe and weighed in pre-weighed vials [39]. Uptake of radioactivity in each sample as well as the background was counted in a well-type γ-counter NaI(Tl). The ^{99m}Tc-Dox-AuNPs uptake per gram of fluid, organ and tumor (% ID/g) were calculated as a fraction of injected dose from the following Eq. (4) [40]:

$$\%\ \mathrm{ID/g\ of\ fluid/organ} = \frac{\text{Radioactivity of tissue or fluid} \times 100}{\text{Total injected radioactivity} \times \text{Weight of tissue or fluid(g)}} \quad (4)$$

The % ID/g expressed the drug concentration in blood, organ and tumor. The maximum % ID/g of ^{99m}Tc-Dox-AuNPs Cmax, %/g) per gram of tumor and its corresponding time (Tmax, h) were determined directly from the biodistribution data. Tumor targeting efficiency was based on the Tumor/Blood (T/B) ratio [41, 42] and drug targeting efficiency percentage (% DTE) that determine the accumulation percent in tumor following intratumoral injection vs. intravenous injection as in the following Eq. (5) [43]

$$\%\ \mathrm{DTE} = ((\mathrm{Tumor_{IT}}/\ \mathrm{Blood_{IT}})/(\mathrm{Tumor_{IV}}/\mathrm{Blood_{IV}})) \times 100 \quad (5)$$

The delivery of [^{99m}Tc]Tc-Doxorubicin to the tumor is associated to % DTE > 100% [43] and tumor/blood ratio > 1 [42].

Statistical analysis

Statistical analysis was done for all obtained result by using SPSS® software version 20 (SPSS Inc., Chicago, USA). One-way analysis of variance (ANOVA) and least-significant difference (LSD) test were applied at level of significance difference $p < 0.05$.

Result and discussion

Preparation of gold nanoparticles delivery system (citrate-reduced gold nanoparticles)

A delivery system of **citrate-reduced gold nanoparticles** (citrate-AuNPs) was prepared through a modified Turkevich method. It was prepared by reduction of hydrogen tetrachloroaurate ($HAuCl_4$) with trisodium citrate ($Na_3C_6H_5O_7$) that acts as a reducing and stabilizing agent [8]. Citrate-AuNPs was successfully prepared by placing 1 ml of 3 mM $HAuCl_4$ solution on heat magnet stirrer at 100 °C and 500 rpm. Immediately after boiling, 1 ml of 1%

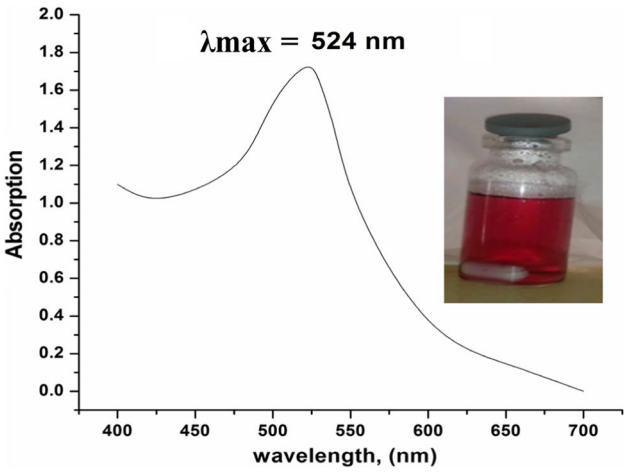

Fig. 2 UV–visible spectroscopy of Citrate-AuNPs

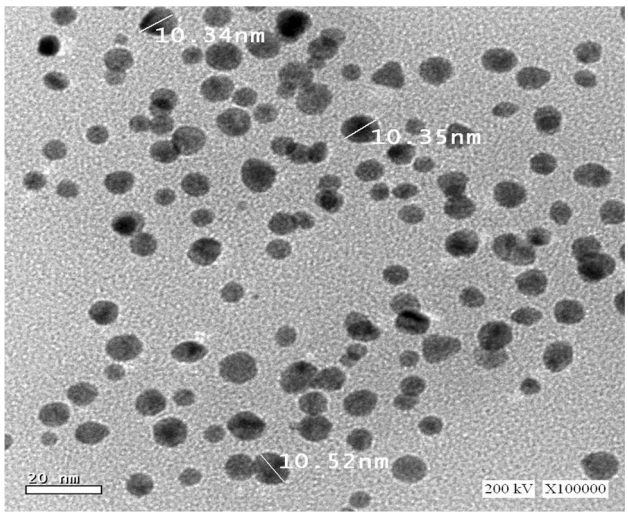

Fig. 3 TEM image of Citrate-AuNPs

trisodium citrate was added with continuous stirring up to 10 min and appearance of a ruby red color.

In vitro characterization of citrate-gold nanoparticles

Identification of citrate-gold nanoparticles:

The delivery system of citrate-AuNPs was screened using UV–visible spectroscopy for determination the wavelength of maximum absorption (λmax). The gold nanoparticles have a special optical phenomenon based on gold nanoparticle particle size and shape as mentioned before. The Aryal et al., 2009 and Liu et al., 2018 [44, 45] were reported that the gold nanoparticles in spherical shape showed maximum absorption (λmax) at 517–530, 540 and 575 nm for spherical size 10–22, 50 and 100 nm, respectively. Figure 2 showed the strong absorption peak for citrate-AuNPs at λmax = 524 nm. The formulations of ^{99m}Tc-Doxo-AuNPs (F1 and F2) were UV screened and detected the absorption peak of citrate-AuNPs at 524 nm and disappearance the characteristic peak of doxorubicin in water at 490 nm [46]. This might be as result of the

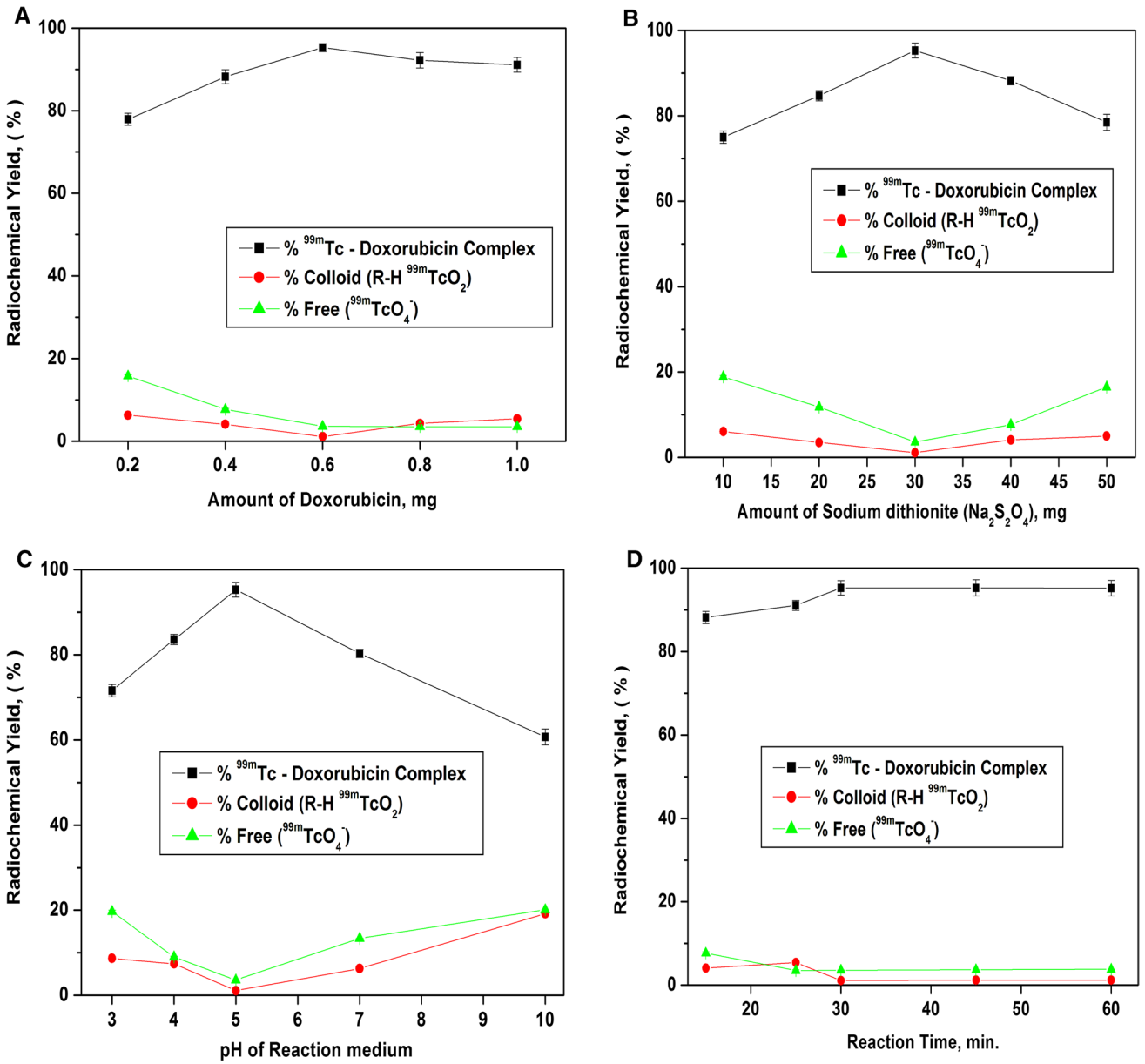

Fig. 4 Variation of radiochemical yield % of ^{99m}Tc-Dox complex as a function of (**A**) doxorubicin amount, (**B**) Reducing agent amount, (**C**) pH, (**D**) Reaction time

overlapping of citrate-AuNPs [47] and confirming that the particle size not change after loading procedure which will confirm by TEM. The stability of ^{99m}Tc-Dox-AuNPs (F1 and F2) at room temperature were confirmed by storage for 4 months; there is no observed change in λmax.

Determination of particle size (PS), polydispersity index (PDI), and zeta potential (ZP)

Characterizations of gold nanocarriers with respect to morphological characteristics, particle size and zeta potential, are very critical to control their desired in vitro and in vivo behavior. The hydrodynamic diameter of citrate-AuNPs was ≈ 20.3 nm. The PDI values were less than 0.5 that could be within the acceptable range [48]. The zeta potential of citrate-AuNPs was – 17.6 mV indicating considerable physical stability with no expected aggregation as a result of electrostatic repulsion between gold nanoparticles produced by the highly negative surface charges [49].

Morphologic examination

Photomicrograph of citrate-AuNPs was illustrated in Fig. 3. It showed that the developed citrate-AuNPs was formed small sized spherical gold nanoparticles varying in their core sizes with a mean of ≈ 10.3 nm comparable that obtained by Zetasizer.

Preparation of radiolabeled Doxorubicin (^{99m}Tc-Dox complex)

The [^{99m}Tc]Tc-Doxorubicin complex was successfully prepared in maximum radiochemical yield (95 ± 0.6%) by direct labeling technique as shown in Fig. 4 at pH 5 using 0.6 mg doxorubicin, 30 mg of sodium dithionite and 100 µl

Table 2 The loading capacity and entrapment efficiency % (EE %) of doxorubicin (DOX) in citrate-AuNPs for different formulations

Formulation of ^{99m}Tc-Dox-AuNPs	Free DOX concentration (mg/ml)	Loading capacity (mg/mg)	Loading efficiency (%)
F1	0.008	0.092	92.3
F2	0.01	0.09	90.1

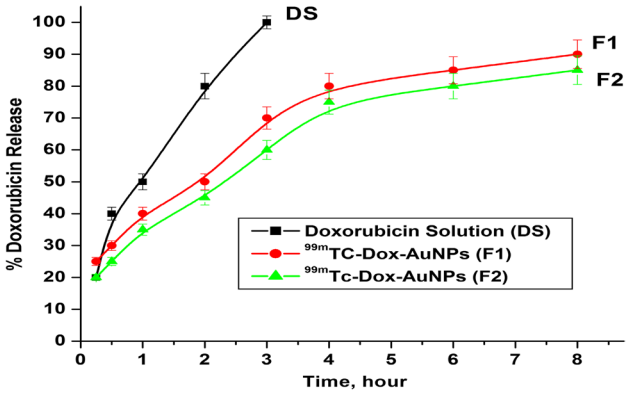

Fig. 5 In vitro drug release profiles from Drug Solution (DS) and ^{99m}Tc-Dox-AuNPs formulations (F1 and F2)

[^{99m}Tc]TcO_4^- for 30 min reaction time at ambient temperature 25 °C. The ^{99m}Tc-Dox complex was stable up to 24 h.

Formulation of ^{99m}Tc-Dox-AuNPs

The formulations of ^{99m}Tc-Dox-AuNPs (F1 and F2) were differed in loading procedure. F1 was prepared by direct formulation method through loading of 0.1 ml prepared [^{99m}Tc]Tc-Doxorubicin complex (1.5 mg/ ml) with 1 ml citrate-AuNPs but F2 was prepared by separately loading 0.15 ml of doxorubicin solution (2 mg/ml) and 100 µl [^{99m}Tc]TcO_4^- with 1 ml citrate-AuNPs. The loading process was done at room temperature and pH 5 with continuous magnet stirrer for 30 min without change in its color or compromising its stability. The obtained radiochemical yields after filtration through sterile millipore filter (0.2 mm) were ≈ 99%.

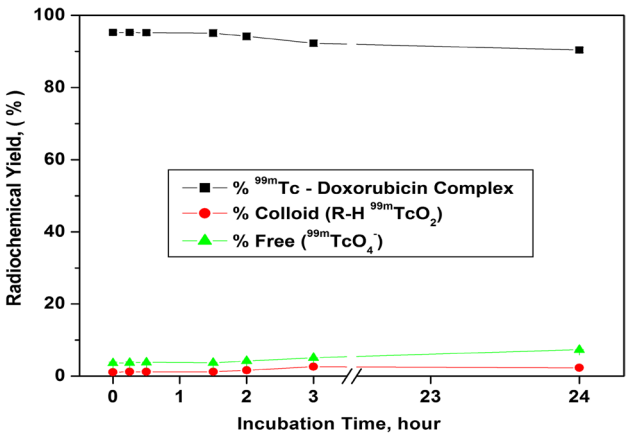

Fig. 6 In vitro stability of ^{99m}Tc-Dox-AuNPs formulations (F1 and F2) in mice serum

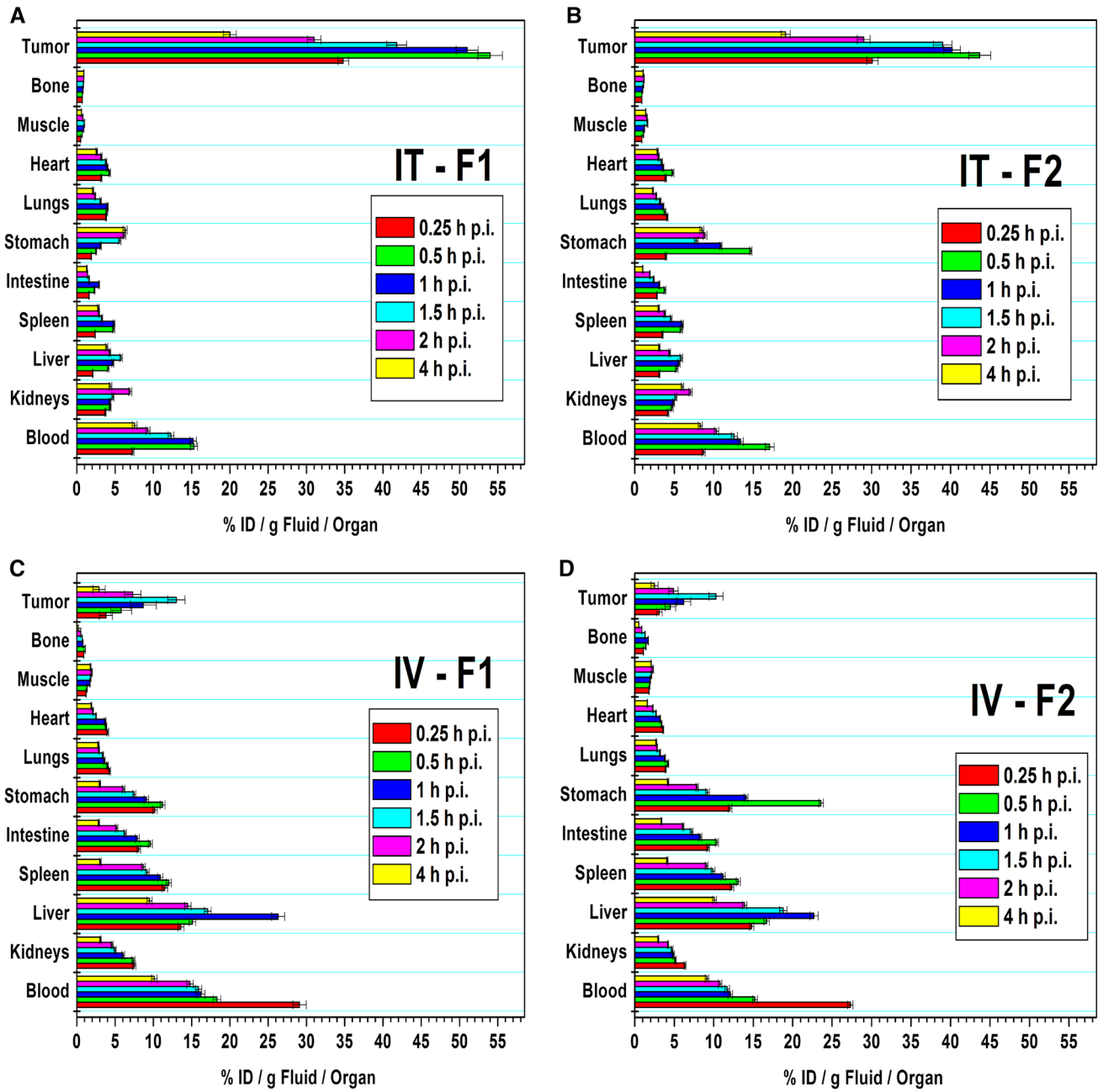

Fig. 7 The comparative in vivo biodistribution of ^{99m}Tc-Dox-AuNPs (F1 and F2) in solid tumor bearing mice following IT and IV injection where (**A**) is IT-F1, (**B**) is IT-F2, (**C**) is IV-F1and (**D**) is IV-F2

In vitro evaluation of formulated ^{99m}Tc-Dox-AuNPs

Determination of loading capacity and entrapment efficiency

As shown in Table 2, the loading capacity for F1 and F2 were 0.092 ± 0.01 and 0.09 ± 0.01 mg/mg, respectively and the entrapment efficiency for F1 and F2 were 92 ± 0.7 and 90 ± 0.3%, respectively. All of these indicate a high ability of citrate-AuNPs to incorporate free doxorubicin or even [^{99m}Tc]Tc-Doxorubicin complex as a result of small size of citrate-AuNPs that permitting for the electrostatic interaction between protonated amino acid of doxorubicin with negatively charged carboxylate groups of citrate [50, 51]. The loading process of doxorubicin could be done by different mechanism (encapsulation, diffusion or surface charges) based on physical, non-covalent or covalent bonding [52, 53].

In-vitro release study

Monitoring doxorubicin release from ^{99m}Tc-Dox-AuNPs formulations (F1 and F2) and drug solution (DS) was done in phosphate buffer solution (pH 5) to mimic the acidic tumor microenvironment. pH value of tumor exhibits lower acidity than pH of normal tissue which might lead to better tumor targeting and drug release for these formulations [54]. In vitro doxorubicin cumulative release profile is shown in Fig. 5. The doxorubicin release from drug solution was used as a control. It showed fast and complete release (100%) within 3 h, this indicates that the doxorubicin could freely diffuse through semi-permeable membrane [55]. The citrate-AuNPs displayed biphasic release; first, doxorubicin was released from the core shell after 15 min at 25 and 20% for F1 and F2, respectively. The time required to release 50% of doxorubicin (t_{50}) from ^{99m}Tc-Dox-AuNPs formulations (F1 and F2) was 2 and 2.5 h, respectively. Second, doxorubicin was slowly released from the core [56]; it was released at 90 and 85% for F1 and F2, respectively after 8 h (Q8h). The results investigate that the citrate-AuNPs could be the best delivery system for ^{99m}Tc-Dox as it not only incorporate a reasonable amount of doxorubicin, but also sustained its release. The biphasic release of doxorubicin may be caused by acidic pH surrounding the tumor cells that reduces the electrostatic interaction between the protonated amino acid of doxorubicin with negatively charged carboxylate groups of citrate [57].

In-vitro stability studies in mice serum

The in vitro stability of ^{99m}Tc-Dox-AuNPs formulations (F1 and F2) in serum play important role in indicating the in vivo stability and the potentiality of delivery system. The in vitro stability of F1 and F2 was assessed in mice serum by paper chromatography at predesigned time up to 24 h. As shown in Fig. 6; F1 showed convenient in-vitro stability in serum up to 24 h. The radiochemical yield of F1 slightly decreased by 4.9% at 24 h but remained significantly higher than radiochemical yield ($83 \pm 0.9\%$) of F2 at 24 h. F2 showed gradient decrease in *in-vitro* stability and increase the free [^{99m}Tc]TcO_4^-, the radiochemical yield reached to $89 \pm 0.4\%$ at 3 h with free [^{99m}Tc]TcO_4^- ($11 \pm 0.2\%$). The radiochemical yield of F2 decreased in serum by 15% at 24 h. This decreasing in in-vitro stability in serum of F2 may effect on its biodistribution behavior and kinetic parameters.

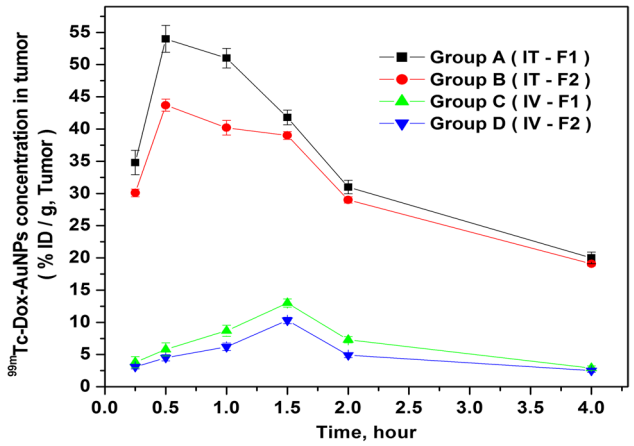

Fig. 9 ^{99m}Tc-Dox-AuNPs concentration in tumor following IT and IV injection

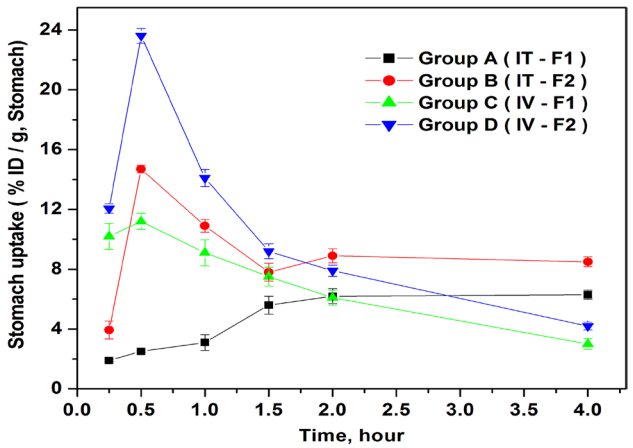

Fig. 8 The comparative uptake of stomach for ^{99m}Tc-Dox-AuNPs (F1 and F2) following IT and IV injection

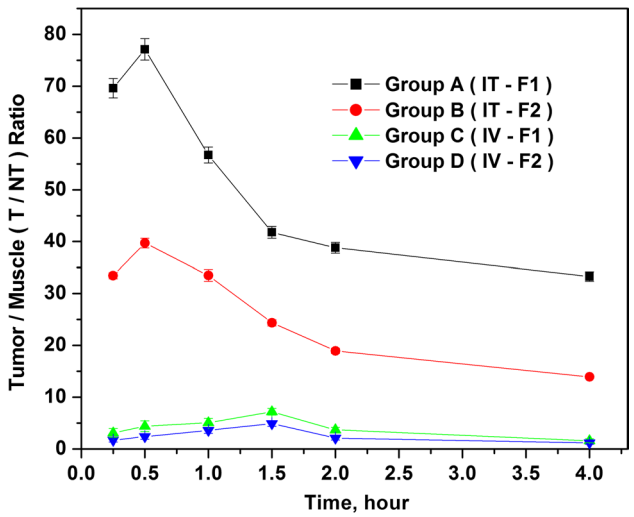

Fig. 10 Target to Non target (T/NT) ratios of ^{99m}Tc-Dox-AuNPs formulations

Table 3 % Drug Targeting Efficiency (% DTE) of ^{99m}Tc-Dox-AuNPs formulations

Time (h)	F1			F2		
	T/B_{IT}	T/B_{IV}	% DTE	T/B_{IT}	T/B_{IV}	% DTE
0.25	4.8	0.13	3692	3.5	0.11	3181
0.5	3.5	0.32	1093	2.6	0.29	897
1	3.4	0.54	629	3	0.51	588
1.5	3.4	0.81	419	3.1	0.88	352
2	3.3	0.49	673	2.8	0.45	622
4	2.7	0.28	964	2.3	0.27	851

Biodistribution studies

The in vivo biodistribution comparative studies represent a great helpful for determination of pharmacokinetics and in vivo stability for F1 and F2 following different route of injection. The biodistribution studies of ^{99m}Tc-Dox-AuNPs were designed in four experimental groups; group A for IT-F1, group B for IT—F2, group C for IV—F1 and group D for IV—F2 as shown in Table 1. The percentage of ^{99m}Tc-Dox-AuNPs concentration per organs, blood and tumor (% ID/g ± SEM) were calculated at predesigned time profile (0.25–4 h) post injection for F1 and F2 via IT (A and B) and IV (C and D), respectively in tumor bearing Swiss albino mice. The comparative biodistribution results are presented in Fig. 7a–d and explained that; following intravenous injection, significantly higher liver accumulation was achieved at 1 h post injection for F1 and F2 (26 ± 0.6 and 23 ± 0.3% ID/g, respectively) that confirms the hepatobiliary pathway of doxorubicin [58]. Following intratumoral injection, it was observed the lower blood levels of ^{99m}Tc-Dox-AuNPs at 0.25 h post injection for F1 and F2 (7 ± 0.32 and 8 ± 0.71% ID/g, respectively). These lower blood levels of ^{99m}Tc-Dox-AuNPs following intratumoral injection are desirable to control systemic side effects of the doxorubicin as cardiac side effect following IV injection [11, 59].

In Fig. 8, It is worth to note the significantly higher stomach uptake at 0.5 h post IT and IV injection of F2 (14 ± 0.86 and 23 ± 0.81% ID/g, respectively) than F1 (2 ± 0.53 and 11 ± 0.3% ID/g, respectively). The high stomach uptake may be the result of escaping of free [^{99m}Tc]TcO_4^- from F2 formulation and this reflect the lower in vivo stability of F2 following IT and IV injection [60].

Following intratumoral injection, significantly lower ^{99m}Tc-Dox-AuNPs (F1 and F2) concentrations were detected in blood, liver and stomach tissues at all-time points. On the other hand intratumoral injection resulted in significantly ($p < 0.05$) faster time (Tmax, 0.5 h post IT injection vs. 1.5 h post IV injection for F1 and F2) to reach ^{99m}Tc-Dox-AuNPs maximum tumor levels (Cmax, 54 ± 0.21% ID/g for F1 and 43 ± 0.1% ID/g for F2 at 0.5 h post IT injection vs. Cmax, 13 ± 0.00% ID/g for F1 and 10 ± 0.4% ID/g for F2 at 1.5 h post IV injection) as shown in Fig. 9 Particularly at early time point 0.5 h, the greater tumor ^{99m}Tc-Dox-AuNPs concentration was determined following intratumoral injection of F2. These results of tumor accumulation following intravenous injection may be based on active ^{99m}Tc-Dox delivery by citrate-AuNPs as a result of interaction between doxorubicin and tumor receptor and passive ^{99m}Tc-Dox delivery that could be related to permeability and retention of small sized of citrate-AuNPs but the tumor accumulation following intratumoral injection were based on localized ^{99m}Tc-Dox delivery system [61, 62].

Comparing the calculated T/NT (%ID/g tumor to %ID/g muscle) ratio following intratumoral and intravenous injection were explained in Fig. 10, it can be observed that; the T/NT at 0.5 h post IT injection of F1 (77 ± 0.4) are significantly higher ($p < 0.05$) than F2 (43 ± 0.84) and also the T/NT at 1.5 h post IV injection of F1 (7 ± 0.29) are significantly higher ($p < 0.05$) than F2 (5 ± 0.1) this reflect the selectivity of F1 via intratumoral injection. This could be related to the extension of the interstitial gaps of tumors based on doxorubicin-induced apoptosis [63, 64].

The tumor targeting efficiency and tumor to blood ratios for ^{99m}Tc-Dox-AuNPs formulations (F1 and F2) were detected at each time point after IT and IV injection as shown in Table 3. Intratumoral injection resulting in a high tumor/blood (T/B) ratio that decreased by time but remained above 1 at all-time points for F1 and F2 however, after IV injection the T/B ratios were below 1 at all-time points for F1 and F2 suggesting high blood rather than tumor. As shown in Table 3, the % drug targeting efficiency (%DTE) were calculated for IT injection of F1 and F2 above 100% at all-time points strongly support the tumor uptake of [^{99m}Tc]Tc-Doxorubicn depending on localized delivery system citrate-AuNPs.

The biodistribution comparative study explained that:

F1 and F2 showed, high brain/blood ratios higher than 1 and % DTE a above 100% specifically at early time points (0.5 h) are evident of rapid and extensive accumulation of [^{99m}Tc]Tc-Doxorubicn in tumor with lower blood uptake prove the potentiality and selectivity of the delivery system (citrate–AuNPs) post intratumoral injection.

F1 of ^{99m}Tc-Dox-AuNPs was 1.24 fold post IT injection and 1.26 fold post IV injection than F2. F1 was 3 times more quickly tumor accumulation at maximum concentration post IT delivery in addition of higher stomach uptake of F2 and therefore the F1 was higher in vivo stability than F2. This prove the loading procedure in formulation may effect on biodistribution and in vivo stability of deliver system in vivo stability of F2.

Finally, the high potentiality and selectivity of ^{99m}Tc-Dox-AuNPs that prepared by direct loading of [^{99m}Tc] Tc-Doxorubicn complex confirm the successful of citrate-AuNPs as a delivery system and ^{99m}Tc-Dox-AuNPs could be used as a imaging agent for solid tumor.

Conclusion

The gold nanoparticles delivery system was synthesized by reduction with citrate ions then functionalized with [^{99m}Tc] Tc-Doxorubicn. The in vivo stability and biodistribution profile of ^{99m}Tc-Dox-AuNPs depending on loading procedure either through direct loading ^{99m}Tc-Dox on AuNPs (F1) or separately loading doxorubicin followed by technithum-99 m (F2). It was found that F1 has higher loading capacity and higher entrapment efficiency than F2 with Q8h = 90% and t_{50} = 2 h. The comparative biodistribution study explained that F1 has better in vivo stability and pharmacokinetics parameters as Cmax ≈ 54%ID/g, lower Tmax (0.5 h), % DTE > 100 and higher T/B ratio > 1 via intra-tumoral (IT) with higher Target/ Non Target ratio (T/NT) of ≈ 77. So, the direct formulation method of ^{99m}Tc-Dox-AuNPs using performed ^{99m}Tc-Dox was a preferable method for preparation and ^{99m}Tc-Dox-AuNPs that could be used as a radiopharmaceutical delivery via IT for tumor diagnosis.

Acknowledgements Associate Prof. Tamer M. Sakr expresses his grateful appreciation and thanks for International Atomic Energy Authority (IAEA), Austria for the international collaboration and funding this work under CRP No. F22064.

Compliance with ethical standards

Conflict of interest The authors declare that they have no known competing financial interests or personal relationships that could have appeared to influence the work reported in this paper.

References

1. Alam Q, Alam MZ, Karim S et al (2014) A nanotechnological approach to the management of Alzheimer disease and type 2 diabetes. CNS Neurol Disord Drug Targets 13(3):478–486
2. Khan AK, Rashid R, Murtaza G, Zahra A (2014) Gold nanoparticles: synthesis applications in drug delivery. Trop J Pharm Res 13(7):1169–1177
3. Tinkle S, McNeil SE, Mühlebach S et al (2014) Nanomedicines: addressing the scientific and regulatory gap. Ann N Y Acad Sci 1313:35–56
4. Shittu KO, Bankole MT, Abdulkareem AS et al (2017) Application of gold nanoparticles for improved drug efficiency. Adv Nat Sci: Nanosci Nanotechnol 8(3):035014
5. Carabineiro SAC (2017) Applications of gold nanoparticles in nanomedicine: recent advances in vaccines. Molecules 22(5):857
6. Gao W, Xu K, Ji L, Tang B (2011) Effect of gold nanoparticles on glutathione depletion-induced hydrogen peroxide generation and apoptosis in HL7702 cells. Toxicol Lett 205(1):86–95
7. Ghosh R, Singh LC, Shohet JM, Gunaratne PH (2013) A gold nanoparticle platform for the delivery of functional microRNAs into cancer cells. Biomaterials 34(3):807–816
8. Turkevich J, Stevenson PL, Hillier J (1951) A study of the nucleation and growth process in the synthesis of colloidal gold. Discuss Faraday Soc 11:55–75
9. Khan S, Alam F, Azam A, Khan AU (2012) Gold nanoparticles enhance methylene blue-induced photodynamic therapy: a novel therapeutic approach to inhibit Candida albicans biofilm. Int J Nanomedicine 7:3245–3257
10. Verma HN, Singh P, Chavan RM (2014) Gold nanoparticle: Synthesis and characterization. Vet World 7(2):72–77
11. Mishra B, Patel BB, Tiwari S (2010) Colloidal nanocarriers: a review on formulation technology, types and applications toward targeted drug delivery. Nanomedicine 6(1):9–24
12. Vigderman L, Zubarev ER (2013) Therapeutic platforms based on gold nanoparticles and their covalent conjugates with drug molecules. Adv Drug Deliv Rev 65(5):663–676
13. Psimadas D, Georgoulias P, Valotassiou V, Loudos G (2012) Molecular nanomedicine towards cancer: ^{111}In-labeled nanoparticles. J Pharm Sci 101(7):2271–2280
14. Papagiannopoulou D (2017) Technetium-99m radiochemistry for pharmaceutical applications. J Labelled Comp Radiopharm 60(11):502–520
15. Kumar P, Singh B, Sharma S et al (2012) Preclinical evaluation of [99m]Tc-labeled doxorubicin as a potential scintigraphic probe for tumor imaging. Cancer Biother Radiopharm 27(3):221–225
16. Kumar P, Singh B, Ghai A et al (2015) Development of a single vial kit formulation of [^{99m}Tc]-labeled doxorubicin for tumor imaging and treatment response assessment preclinical evaluation and preliminary human results. J Label Compd Radiopharm 58:242–249
17. Hendel T, Wuithschick M, Kettemann F et al (2014) In situ determination of colloidal gold concentrations with UV-vis spectroscopy: limitations and perspectives. Anal Chem 86(22):11115–111124
18. Lim SP, Lim YS, Pandikumar A et al (2017) Gold-silver@TiO_2 nanocomposite-modified plasmonic photoanodes for higher efficiency dye-sensitized solar cells. Phys Chem Chem Phys 19(2):1395–1407
19. Kelly KL, Coronado E, Zhao LL, Schatz GC (2003) The optical properties of metal nanoparticles: the influence of size, shape, and dielectric environment. J Phys Chem B 107(3):668–677
20. Scognamiglio I, De Stefano D, Campani V et al (2013) Nanocarriers for topical administration of resveratrol: a comparative study. Int J Pharm 440(2):179–187
21. Abd El-Halim SM, Abdelbary GA, Amin MM et al (2020) Stabilized oral nanostructured lipid carriers of Adefovir Dipivoxil as a potential liver targeting: estimation of liver function panel and uptake following intravenous injection of radioiodinated indicator. Daru 28(2):517–532

22. Fahmy AM, El-Setouhy DA, Ibrahim AB et al (2018) Penetration enhancer-containing spanlastics (PECSs) for transdermal delivery of haloperidol: in vitro characterization, ex vivo permeation and in vivo biodistribution studies. Drug Deliv 25(1):12–22
23. Vilcek S, Kalincák M, Machán V (1981) ^{99m}Tc-labelled compounds prepared with sodium dithionite as reducing agent. Nuklearmedizin 20(6):283–289
24. Ibrahim AB, Shamsel-Din HA, Hussein AS, Salem MA (2020) Brain-targeting by optimized ^{99m}Tc-olanzapine: in vivo and in silico studies. Int J Radiat Biol 96(8):1017–1027
25. Al-Wabli RI, Sakr TM, Khedr MA et al (2016) Platelet-12 lipoxygenase targeting via a newly synthesized curcumin derivative radiolabeled with technetium-99m. Chem Cent J 10(1):73
26. Shamsel-Din HA, Ibrahim AB (2017) A novel radiolabeled indole derivative as solid tumor imaging agent: in silico and preclinical pharmacological study. J Radioanal Nucl Chem 314(3):2263–2269
27. El-Ghareb WI, Swidan MM, Ibrahim IT et al (2020) ^{99m}Tc-doxorubicin-loaded gallic acid-gold nanoparticles (^{99m}Tc-DOX-loaded GA-Au NPs) as a multifunctional theranostic agent. Int J Pharm 586:119514
28. Swidan MM, Khowessah OM, El-Motaleb MA et al (2019) Iron oxide nanoparticulate system as a cornerstone in the effective delivery of Tc-99 m radionuclide: a potential molecular imaging probe for tumor diagnosis. Daru 27(1):49–58
29. Sakr TM, Khowessah OM, El-Motaleb MA et al (2018) I-131 doping of silver nanoparticles platform for tumor theranosis guided drug delivery. Eur J Pharm Sci 122:239–245
30. Balcioglu M, Rana M, Yigit MV (2013) Doxorubicin loading on graphene oxide, iron oxide and gold nanoparticle hybrid. J Mater Chem B 1(45):6187–6193
31. Samia O, Hanan R, Kamal ET (2012) Carbamazepine mucoadhesive nanoemulgel (MNEG) as brain targeting delivery system via the olfactory mucosa. Drug Deliv 19(1):58–67
32. Shamma RN, Elsayed I (2013) Transfersomal lyophilized gel of buspirone HCl: formulation, evaluation and statistical optimization. J Liposome Res 23(3):244–254
33. Barrán-Berdón AL, Pozzi D, Caracciolo G et al (2013) Time evolution of nanoparticle-protein corona in human plasma: relevance for targeted drug delivery. Langmuir 29(21):6485–6494
34. Ibrahim AB, Sakr TM, Khoweysa OM et al (2015) Radioiodinatedanastrozole and epirubicin as potential targeting radiopharmaceuticals for solid tumor imaging. J RadioanalNucl Chem 303(1):967–975
35. Ibrahim AB, Salem MA, Fasih TW et al (2018) Radioiodinated doxorubicin as a new tumor imaging model: preparation, biological evaluation, docking and molecular dynamics. J Radioanal Nucl Chem 317(3):1243–1252
36. Sakr TM, Khedr MA, Rashed HM et al (2018) *In Silico*-Based repositioning of phosphinothricin as a novel technetium-99m imaging probe with potential anticancer activity. Molecules 23:496
37. Mohamed KO, Nissan YM, El-Malah AA et al (2017) Design, synthesis and biological evaluation of some novel sulfonamide derivatives as apoptotic agents. Eur J Med Chem 135:424–433
38. Swidan MM, Sakr TM, Motaleb MA et al (2015) Preliminary Assessment of radioiodinatedfenoterol and reproterol as potential scintigraphic agents for lung imaging. J RadioanalNuclChem 303(1):531–539
39. Swidan MM, Sakr TM, Motaleb MA et al (2014) Radioiodinatedacebutolol as a new highly selective radiotracer for myocardial perfusion imaging. J Labelled Compound Radiopharm 57:593–599
40. Saha GB (1993) In: methods of radiolabeling physics and radiobiology of nuclear medicine, 1st edn. Springer-Verlag, New York, pp 100–106
41. Chow HS, Chen Z, Matsuura GT (1999) Direct transport of cocaine from the nasal cavity to the brain following intranasal cocaine administration in rats. J Pharm Sci 88(8):754–758
42. Yadav S, Gattacceca F, Panicucci R, Amiji MM (2015) Comparative biodistribution and pharmacokinetic analysis of cyclosporine-A in the brain upon intranasal or intravenous administration in an oil-in-water nanoemulsion formulation. Mol Pharm 12(5):1523–1533
43. Kozlovskaya L, Abou-Kaoud M, Stepensky D (2014) Quantitative analysis of drug delivery to the brain via nasal route. J Control Release 189:133–140
44. Aryal S, Grailer JJ, Pilla S et al (2009) Doxorubicin conjugated gold nanoparticles as water-soluble and pH-responsive anticancer drug nanocarriers. J Mater Chem 19(42):7879–7884
45. Liu Y, Crawford BM, Vo-Dinh T (2018) Gold nanoparticles-mediated photothermal therapy and immunotherapy. Immunotherapy 10(13):1175–1188
46. Ranjbar-Navazi Z, Eskandani M, Johari-Ahar M et al (2018) Doxorubicin-conjugated D-glucosamine- and folate- bi-functionalised InP/ZnS quantum dots for cancer cells imaging and therapy. J Drug Target 26(3):267–277
47. Chaudhary A, Dwivedi C, Gupta A, Nandi CK (2015) One pot synthesis of doxorubicin loaded gold nanoparticles for sustained drug release. RSC Adv 5(118):97330–97334
48. Cho HJ, Park JW, Yoon IS, Kim DD (2014) Surface-modified solid lipid nanoparticles for oral delivery of docetaxel: enhanced intestinal absorption and lymphatic uptake. Int J Nanomed 9:495–504
49. Honary S, Zahir F (2013) Effect of zeta potential on the properties of nano-drug delivery systems – a review (Part 2). Trop J Pharm Res 12(2):265–273
50. Raghunand N, Mahoney BP, Gillies RJ (2003) Tumor acidity, ion trapping and chemotherapeutics pHdependent partition coefficients predict importance of ion trapping on pharmacokinetics of weakly basic chemotherapeutic agents. Biochem Pharmacol 66(7): 1219–1229
51. Curry D, Cameron A, MacDonald B et al (2015) Adsorption of doxorubicin on citrate-capped gold nanoparticles: insights into engineering potent chemotherapeutic delivery systems. Nanoscale 7(46):19611–19619
52. Anselmo AC, Mitragotri S (2014) Cell-mediated delivery of nanoparticles: taking advantage of circulatory cells to target nanoparticles. J Control Release 190:531–541
53. Austin LA, Mackey MA, Dreaden EC, El-Sayed MA (2014) The optical, photothermal, and facile surface chemical properties of gold and silver nanoparticles in biodiagnostics, therapy, and drug delivery. Arch Toxicol 88(7):1391–1417
54. Gerweck LE, Vijayappa S, Kozin S (2006) Tumor pH controls the in vivo efficacy of weak acid and base chemotherapeutics. Mol Cancer Ther 5(5):1275–1279
55. Wei Z, Hao J, Yuan S et al (2009) Paclitaxel-loaded Pluronic P123/F127 mixed polymeric micelles: formulation, optimization and in vitro characterization. Int J Pharm 376(1–2):176–185
56. Torchilin V, Amiji MM (2010) In Polymeric micelles as versatile carriers for drugs and nucleic acids delivery (ed) Handbook of materials for nanomedicine. Pan Stanford Publishing, Danvers
57. You J, Zhang G, Li C (2010) Exceptionally high payload of doxorubicin in hollow gold nanospheres for near-infrared light-triggered drug release. ACS Nano 4(2):1033–1041
58. Elbialy NS, Fathy MM, Khalil WM (2015) Doxorubicin loaded magnetic gold nanoparticles for in vivo targeted drug delivery. Int J Pharm 490(1–2):190–199

59. Idani H, Matsuoka J, Yasuda T et al (2000) Intra-tumoral injection of doxorubicin (adriamycin) encapsulated in liposome inhibits tumor growth, prolongs survival time and is not associated with local or systemic side effects. Int J Cancer 88(4):645–651
60. Rashed HM, Marzook FA, Farag H (2016) ^{99m}Tc-zolmitriptan: radiolabeling, molecular modeling, biodistribution and gamma scintigraphy as a hopeful radiopharmaceutical for lung nuclear imaging. Radiol Med 121(12):935–943
61. Kim HS, Lee YS, Kim DK (2009) Doxorubicin exerts cytotoxic effects through cell cycle arrest and Fas-mediated cell death. Pharmacology 84(5):300–309
62. Ruttala HB, Ramasamy T, Madeshwaran T et al (2018) Emerging potential of stimulus-responsive nanosized anticancer drug delivery systems for systemic applications. Arch Pharm Res 41(2):111–129
63. Jang SH, Wientjes MG, Au JL (2001) Determinants of paclitaxel uptake, accumulation and retention in solid tumors. Invest New Drugs 19(2):113–123
64. Zheng JH, Chen CT, Au JL, Wientjes MG (2001) Time- and concentration-dependent penetration of doxorubicin in prostate tumors. AAPS PharmSci 3(2):E15